Int J Adv Manuf Technol (2013) 64:889–901
DOI 10.1007/s00170-012-4041-3

ORIGINAL ARTICLE

Thermal growth measurement and compensation for integrated spindles

Kuen-Hung Hsieh · Tsair-Rong Chen · Paul Chang · Chia-Hui Tang

Received: 28 March 2011 / Accepted: 5 March 2012 / Published online: 14 April 2012

Abstract The errors which affect the processing tolerance of a machine tool are due to the built-in volumetric errors in the machine tool structure and also the thermal displacement of the machine tools during its cutting. In this paper, a dual-displacement meter compensation system is developed. The new model has a better tolerance control than the single-displacement compensation meter method; also, it has a great potential for saving a machine's warm-up time as well as enhancing productivity. A dual-displacement meter is designed to detect the variation of spindle thermal growth and a differential amplifier is applied which ensure a precise output signal tolerance of spindle thermal growth. The unstable signal which is an effect of flatness tolerance of spindle surface is then omitted. Finally, the spindle thermal growth compensations are successfully reduced. It meets the requirement of high-speed machining and high-precision machining application.

Keywords Thermal displacement · Differential amplifier · High-speed machining

1 Introduction

High-speed machining (HSM) technology is used in a broad range of applications to machine aluminum alloys, ferrous metals, and nonmetallic materials [1–3]. (Aluminum alloys are metallic and nonferrous.) Based on its application, an integrated high-speed spindle, which provides large power and torque, is the key core component of HSM. However, with the increase of speed and power of spindle, spindle thermal growth becomes a critical issue to be considered.

The spindle dynamic model is constructed by using finite elements based on Timoshenko beam theory. The thermal growth of the spindle, housing, and bearings are calculated based on predicted temperature distributions and are used to update the bearing preloads depending on the operating conditions. The thermal growth compensation of the spindle is again used to update the thermal model [4–6].

Although a good spindle design with proper bearing preload is widely accepted, but the long working hour and high-spindle speed will cause thermal growth and rapidly increase the loading of bearings by centrifugal force [7–9]; the higher speed of spindle, the higher centrifugal force will be. Figure 1 illustrates a motorized spindle structure. A pair of angular contact ball bearings is used to support the lower portion of the spindle. It is also a proven design and good solution for higher revolution speeds as the angular contact ball bearings are capable of absorbing both axial and radial thrust typical of a normal machining [7, 8].

In Fig. 2, as the load on the bearings increases during a normal cutting from many different directions, the resultant decrease in the gap of bearings will cause nonlinear temperature to rise sharply [9].

Though the spindle was manufactured with the proper preload on the bearings and operated within acceptable parameters, the added loading of the cutting application still causes the spindle thermal growth and unacceptable part finish. Though the spindle bearing are properly preloaded and operated within acceptable parameters, the increased loading of the cutting application still leads to spindle thermal growth and poor surface finish

PT100 platinum thermocouplers [10] has been traditionally applied as it provides reasonably reliable feedback; this

K.-H. Hsieh · T.-R. Chen · P. Chang (✉) · C.-H. Tang
Department of Electrical Engineering,
Chang-hua University of Education,
Changhua, Taiwan, China
e-mail: paulchang@mail.buffalo.com.tw

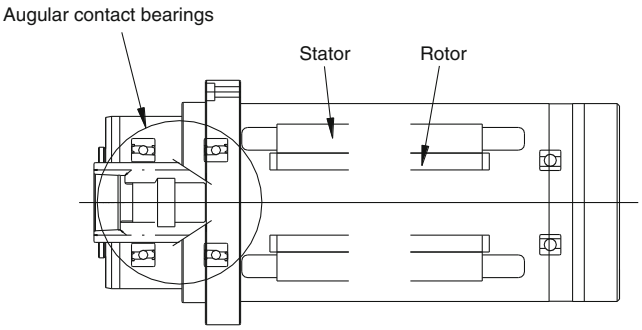

Fig. 1 Motorized spindle structure

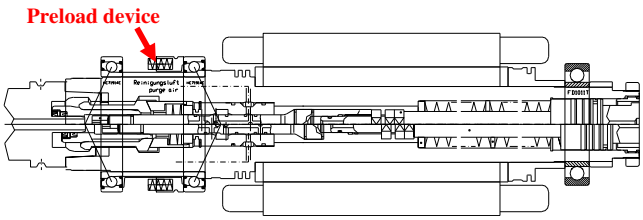

Fig. 3 Motorized spindle with spring preload structure

linear device is usually used in measuring wide range of the temperature rise, seriously varying temperature such as 0–1,000°C. Therefore, for spindle with smoothly varying temperature, PT100 is acceptable but not optimal as it is an indirect measurement. While the thermometer is placed very closely to the front spindle bearings, its measurement inaccuracy still remains.

Based on the theory of Foucault current, this study applies the displacement *t* meter placed in front of the spindle to measure the value of spindle extension. The PLC can compensate the thermal growth of all axes and can feedback quickly with higher accuracy than PT100 thermal coupler. The result show increases the machining accuracy, meets the requirement of HSM technology, and undoubtedly adds the value of the machining tools.

2 Thermal displacement modeling of spindle

This section investigates the effect of spindle thermal growth on tolerance and the design of bearing load control. The characteristics of thermal growth and the restriction of traditional PT100 thermal coupler will be investigated in the future. Besides, this section identifies the characteristic of Foucault current and its application on the spindle growth measurement.

2.1 Bearings loading control

Figure 3 shows a motorized high-speed spindle using spring force to preload the spindle bearings. Most high-speed spindles are designed for high rotational speed in rotations per minute (RPM) and high simultaneous axes feeds for light cutting tool load applications [7, 8]. A piezoelectric actuator has been placed behind the spindle to maintain proper bearing loading. Shown in Fig. 4, the front spindle bearings is considered to be of the traditional design which still induces greater heat with the increase of spindle speed and running hour.

2.2 Characteristic of thermal growth

Figure 5 outlines the thermal growth of a motorized high-speed spindle running at different RPM for a constant time. All thermal growth curves are not parallel and the differences between all curves are not identical. Each thermal growth curves are not parallel and nonlinear (see A and B) A constant compensation parameter will not improve its performance [11, 12].

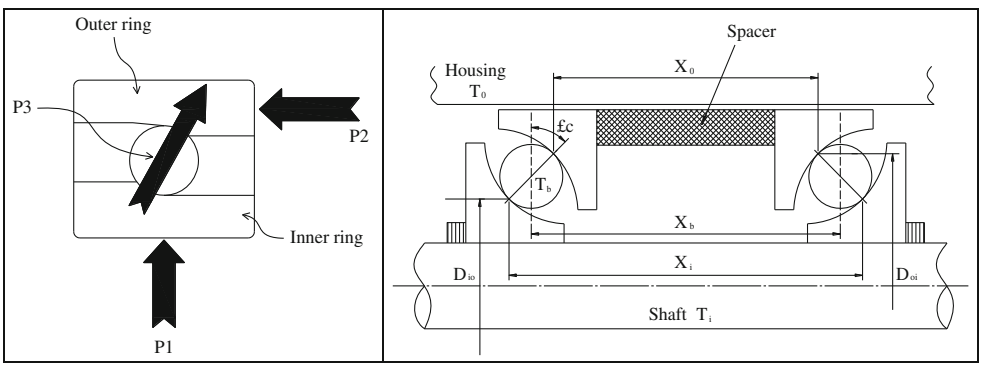

Fig. 2 *Left* bearing pressures from different directions; *right* preload mechanism

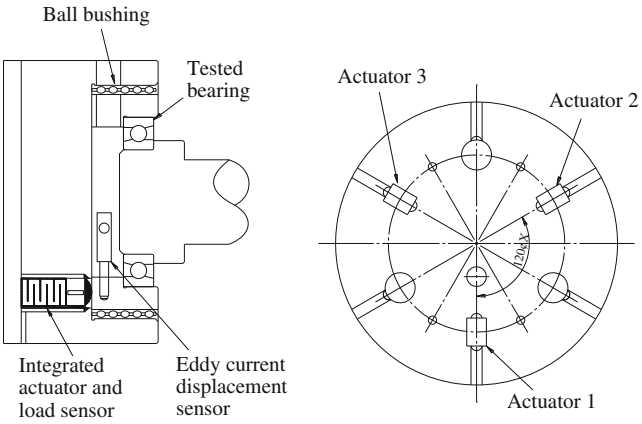

Fig. 4 Spindle bearings with actuator

2.3 Foucault current

Foucault current (also known as eddy current) is a phenomenon discovered by a French physicist named Leon Foucault [13–17]. It defines that a moving conductor changes in the magnetic field generated by stationary objects, the relative motion will cause a circulating flow of electrons or current. Faradays law outlines the equation as below:

$$V_L = L\frac{d_i}{d_t} \tag{1}$$

where

V_L is the induced voltage in volt
L is the value of inductance in henries
$\frac{d_i}{d_t}$ is the rate of the current change in ampere per second

It is very important to know the characteristic of the current penetration depth and current density. Figure 6 presents the penetration, which shows a narrow range of data to be measured.

This penetration depth is given by:

$$\delta \approx \frac{1}{\sqrt{\pi f \mu \sigma}} \tag{2}$$

where

f is the test frequency, which is 50 or 60 Hz
μ is the magnetic permeability of the spindle in henries per meter
σ is the electrical conductivity of the spindle in siemens per meter

In this research, the material used for these spindles is chromium molybdenum steel (grade 4,140), with a magnetic permeability of 750 H/m and the electrical conductivity is set $9.8^{10^{-5}}$ S/m. Thus, the penetration depth of the spindles can be calculated by using Eq. (2), and has the value of 0–3 mm.

2.4 Single displacement measurement meter

Based on the law of Foucault current (Eddy current) and Faraday law, a displacement measurement meter is developed as shown in Fig. 7. It provides a much precise result of spindle thermal growth. The meter measures spindle expansion directly, and the voltage is a perfect linear output [13–15, 17].

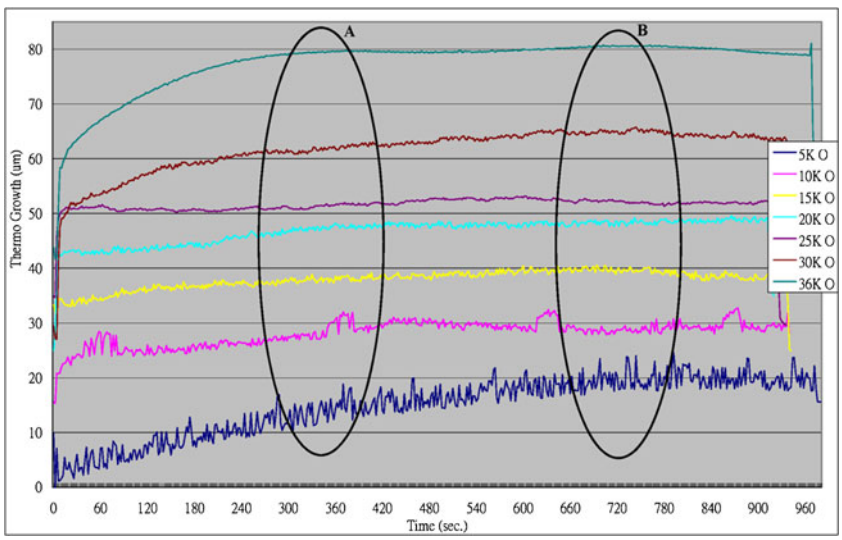

Fig. 5 Temperature raise vs. spindle speed

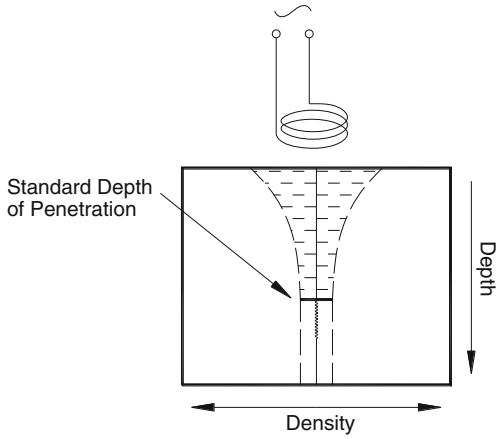

Fig. 6 Penetration of Foucault current [14]

2.5 Single displacement meter compensation

The controlling flowchart of single-measurement meter for thermal growth of spindle is shown in Fig. 8.When the expansion of spindle is 1 μm, the output voltage is defined as 20 mV. The boundary condition is $V_n = V_o - V_r$, where V_r is the reference value of voltage and V_o is the incremental voltage from thermal growth of spindle [18–26].

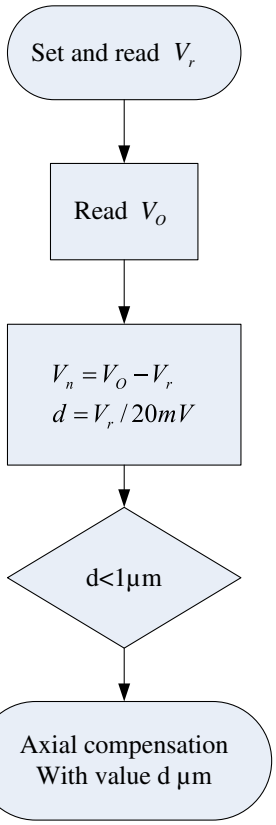

Fig. 8 Flowchart of single-measurement meter

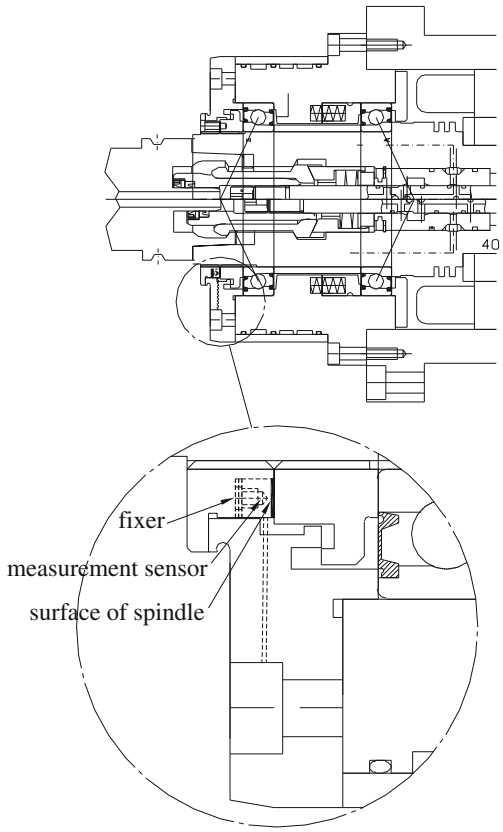

Fig. 7 Spindle with single-displacement meter

The compensation value of thermal growth is d, where $d = V_r/20$ mV, its unit is 1 μm. If the difference between output voltage and reference voltage is less than 20 mV, the compensation for thermal growth will not be implemented by the controller. In contrast, the negative compensation for axes by d μm will be activated when the difference between output voltage and reference voltage is larger or equal to 20 mV. The simplified diagram is shown as Fig. 9.

The input voltage V_i is detected by the distance variance of displacement measurement meter. The relationship between input current i of amplified circuit and impedance z can be expressed as:

$$\frac{1}{z} = \frac{1 + j\omega R_2 C_1}{R_2} \tag{3}$$

or

$$z = \frac{R_2}{1 + j\omega R_2 C_1} \tag{4}$$

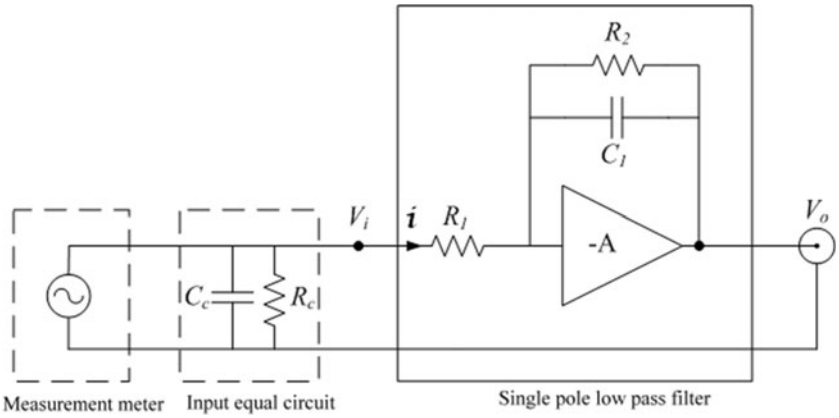

Fig. 9 Single-measurement meter operational amplified circuit

In Eqs. (3)–(4), z is the parallel impedance of C_1 and R_2.

$$i = \frac{V_i}{R_1} \tag{5}$$

$$V_0 = -i \cdot z = -\frac{V_i}{R_1} \cdot z = -\frac{V_i}{R_1} \cdot \frac{R_2}{1 + j\omega R_2 C_1} \tag{6}$$

Input voltage and output voltage can be expressed as Eq. (6)

2.6 Simulation of single-displacement meter

Figure 10 shows the amplifier diagram of single-displacement measurement meter. The amplifier is a single-pole low-pass filtering device. In Fig. 10, V_1 is the testing power supply, RL is the load resistor. Resistor R_1 and R_2 is for changing voltage gain of low frequency. Bandwidth can be adjusted by capacitor C_1 and resistor R_2. The simulation is based on the following data: R_1=10 K, R_2=10 K, C_1=1.6 nF, and RL=10 K.

Figure 11 shows the Bode plot of frequency versus output voltage, it indicates that the voltage is a stable output between 0 and 1 kHz, reflecting that the amplification ratio will not change within this range. Thus, we can find the bandwidth is 10 kHz, which meets the requirement of the application.

Figure 12 is the Bode plot of frequency versus phases and illustrates the phase differential of input and output voltage is 180° when the frequency is under 300 Hz. From the view of mechanic physical structure, the bandwidth is quite large for normal mechanical structure. As a result, the bandwidth of the amplifier fits the measurement demand of spindle thermal growth compensation.

Figure 13 shows a comparison of spindle growth versus laser measurement value. It is clear that spindle growth matches the laser report after the spindle running for 4,200 s. It meets the requirement of high-speed spindle that normally runs at high-speed range. But point C and point d still show a difference of 7.5 and 3 μm due to a measuring error.

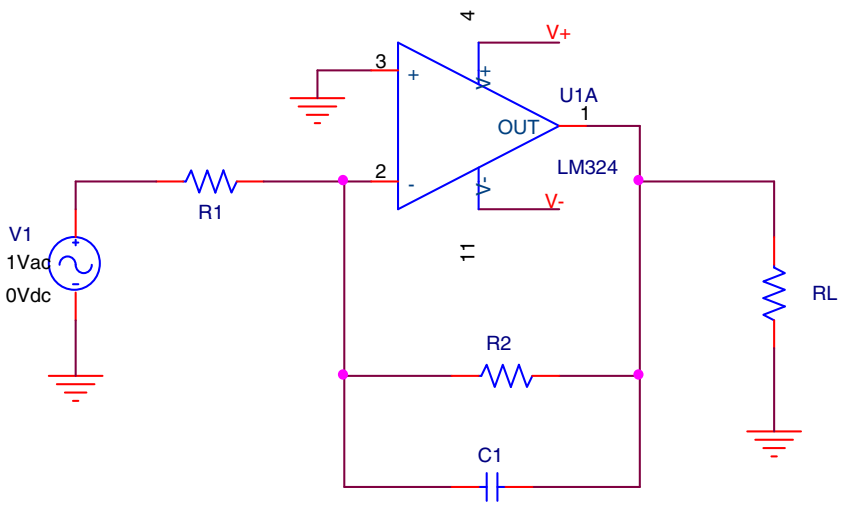

Fig. 10 Single-measurement meter simulation diagram

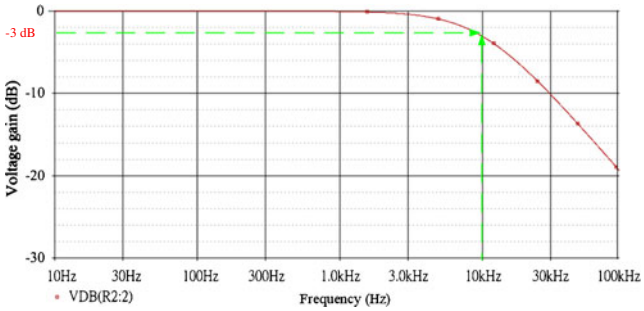

Fig. 11 Single-measurement meter voltage gain Bode plot

3 Model development (dual-measurement meters)

3.1 Mechanical design

This new model consists of dual pieces of measurement meters placed in front of the spindle [18, 19]. Single meter is used as a reference and the other one is used to measure 3–5 mm away, depending on the space and its rigidity of the spindle end cover. Both meters should be fitted very closely, facing to the spindle end upright, and all geometrical distance between 2 m should be as close as possible. The geometrical tolerance is then reduced to the smallest. The differential amplifier is then applied. Figure 14 shows the meters placed on the bottom cover of spindle.

3.2 Logic concept and amplifier

To get a perfect performance of cutting result, the compensation logic has been set to allow the spindle axis compensation of every ±1 μm when the output voltage changes per ±0.02 v. The flow chart is shown in Fig. 15.

3.3 Simulation of dual-measurement meters

The circuit diagram of the dual-measurement amplifier circuit is shown in Fig. 16, it is a differential amplifier. The two

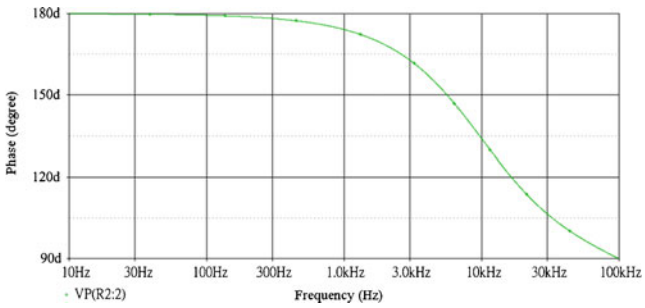

Fig. 12 Single-measurement meter phase Bode plot

voltages V_1 and V_2 represent the output voltages of the measurement devices. The voltage gain can be adjusted by changing the resistance values of R_1, R_2, R_3, and R_4. In this study, the resistance R_3 is set equal to R_4.

One of the meters is used as a reference; the second meter is mounted 3 mm lower from the reference meter, this is the measuring meter. It provides a significant improvement of its measuring error [21].

where:

V_{in1}	is the input voltage reading from the reference meter
V_{in2}	is the input voltage reading from the displacement meter
R_6	is a ratio resistor, rated four or two times
R_1, R_3	are input circuit insulation resistors
R_2	is the time control resistor

And the equation is given as following:

$$i = \frac{V_{in2} - V_{in1}}{R_1} = \frac{V_{dif}}{R \cdot \mathrm{Sin}\omega t} \tag{7}$$

where

ωt	is the phase angle at time t
V_{in1} and V_{in2}	are the input voltages

To investigate the frequency response of the amplifier circuit, the gain and phase Bode plot of the amplifier are presented by utilizing the simulation software. In the simulation, the input voltages V_1 and V_2 are set identical and the data in Bode plot are normalized. The respective parameters of the devices are R_1=1 k, R_2=500Ω, R_3= 1 k, and R_4=1 k.

Figure 17 shows the Bode plot of the voltage gain of the amplifier circuit. It demonstrates that the 3 dB bandwidth of the circuit is about 10 kHz which is perfectly suitable for the displacement measurement meter.

From Fig. 18, one can see that the output voltage is nearly in phase with the input voltage with the frequency lower than 300 Hz. Therefore, from the simulation results, the design of the amplifier circuit obviously meets the requirement of the displacement measurement meter. Due to the same type of single-pole low-pass filter used, the simulation results are nearly the same as the single-displacement measurement meter. Although the frequency response of the dual-displacement measurement meter is similar to the single-type meter, the accuracy of the displacement measurement can be further doubled.

3.4 Control system

The control system is used to measure the output voltage; it can be designed to be a reference level which

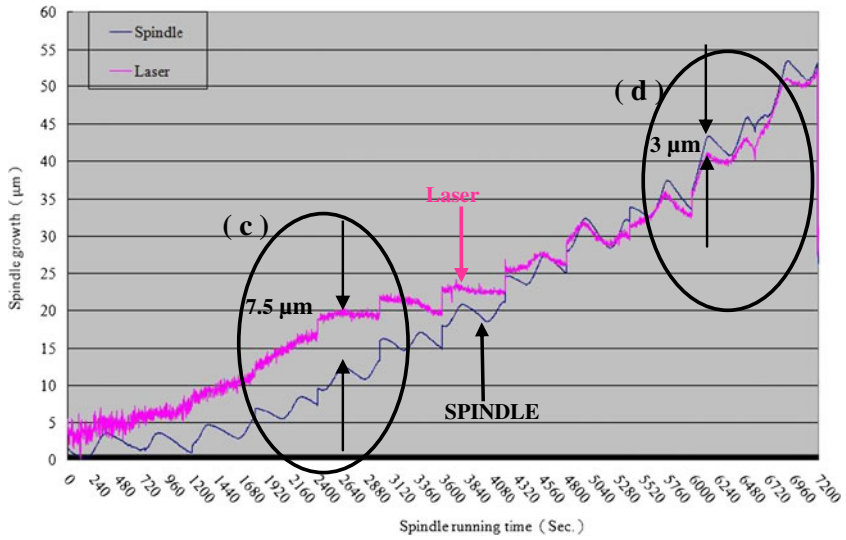

Fig. 13 Spindle growth versus laser report

links to the designed scale of the CPU control system. An M-Code reference has been designed to measure output voltage in sequence. It includes definition of sequence times, analog signal for CPU, and reset measurement process. The system will control when the spindle growth is within tolerance or output voltage is larger than constant value *K*. Then, the voltage is converted to a compensation value as set in Fig. 15 flowchart. The M-code sample is shown in Fig. 19.

3.5 Precheck device

The displacement measurement meter could be moved after long-time usage and some occasional accidents such as crash from improper operation. Thus, the position detection of the displacement meter when starting the machine and after initial installation is necessary. Considering the temperature sensitivity of the displacement measurement meter, this study fitted a temperature

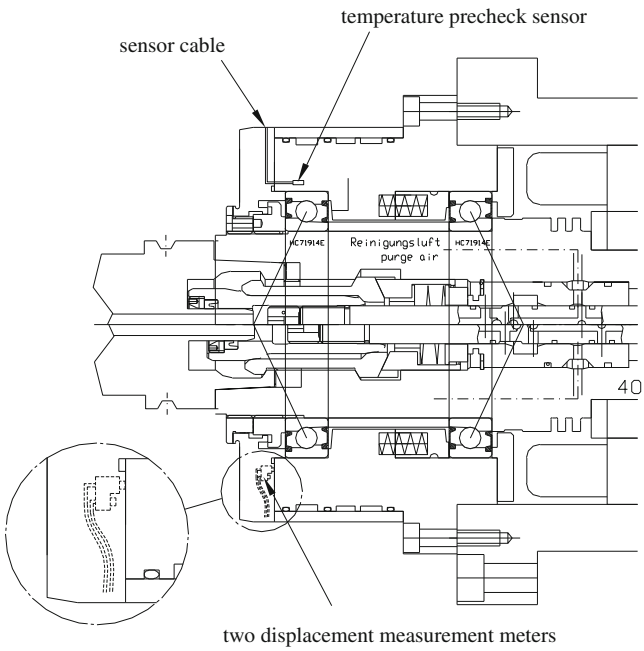

Fig. 14 Spindle with dual-displacement measurement meters

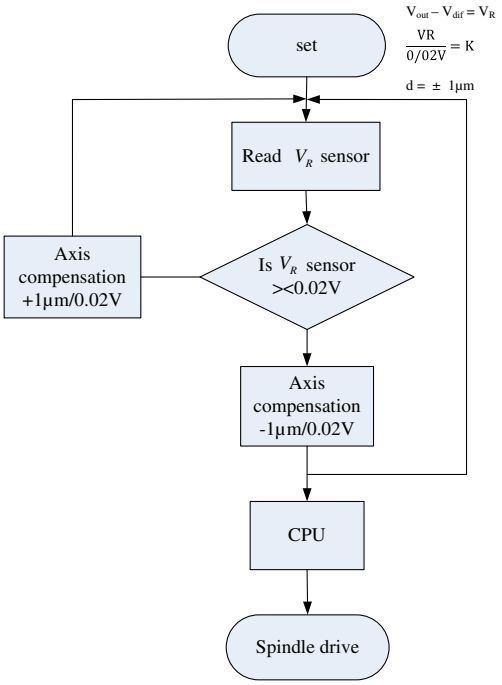

Fig. 15 Flowchart of dual-measurement meter

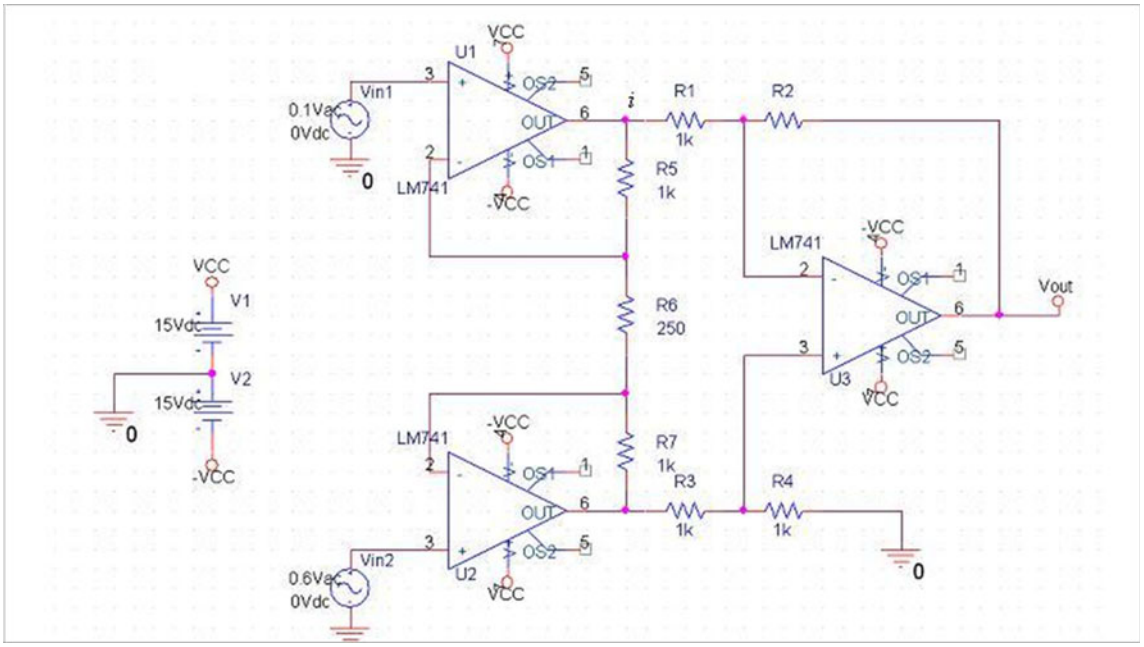

Fig. 16 Differential amplifier diagram

sensor in the opposite side (180°) of the displacement meter. To avoid the temperature effect on accuracy, the temperature sensor is used for compensating the temperature of displacement meter.

Figure 20 shows the flowchart of designing displacement measurement meter. The flowchart ensures the sensor can be reset and compensate precisely within acceptable tolerance or even over the tolerance after operation.

Where

(14–1) Define the checking sequence, sample is set 100 times each pulse width
(14–2) Stop compensation when PLC is not started or CPU is receiving input
(14–3) Analog signal processor in CPU
(14–4) Output voltage summary
(14–5) Reset after CPU receive every input
(14–6) Voltage value counting (RMS)
(14–7) Voltage convert to be distance
(14–8) Reset

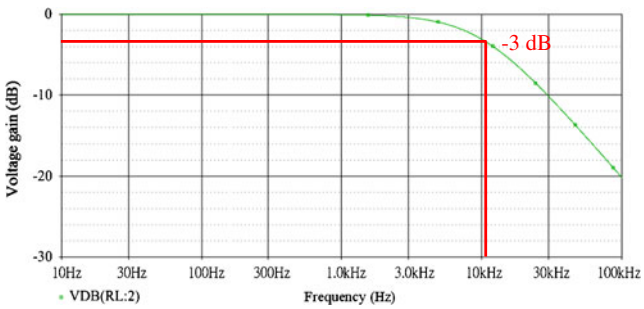

Fig. 17 Dual measurement meter voltage gain Bode plot

4 Experiment and performance

4.1 Amplifier experiment

To assure the quick and accurate measurement of voltage gain and phase, a high-frequency response checking equipment (Model TF-2000) made by Voltech Instrument is used in this study. For the accuracy and reliability of the amplifier designs in this study, the voltage gain and phase testing will be testified in this section.

4.1.1 Experimental results and discussions of the single-displacement measurement meter

The gain and phase bold plots of the amplifier circuit of the single-displacement measurement meter are shown in Figs. 21 and 22. The experimental results show that the design fit the bandwidth requirement. The increase of the voltage gain at about 100 kHz may result from the effect of the stray capacitance and inductance in the circuit or the nonlinearity of the operation amplifier. However, this effect can be neglected because the designed circuit is not used in the high-frequency region. Also, comparing

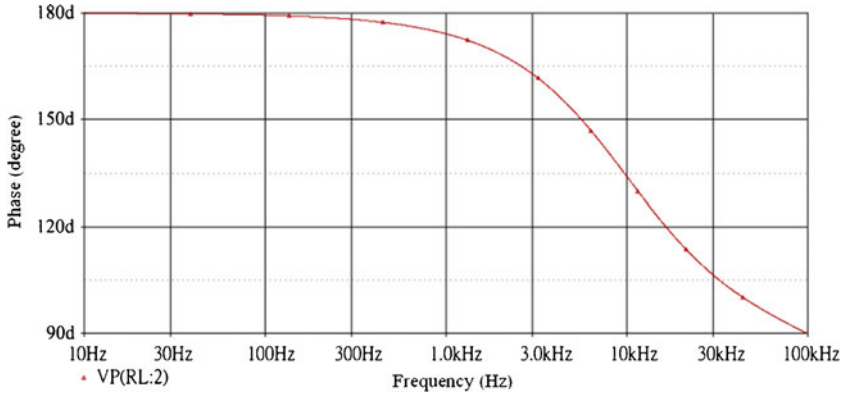

Fig. 18 Dual-measurement meter phase Bode plot

with the simulation results with PSpice, Figs. 11 and 12, the characteristic curves are nearly the same. It is obvious that the designed amplifier circuit is perfectly suitable.

4.1.2 Experimental results and discussions of the dual-displacement measurement meter

The testing procedures of the dual-displacement measurement meter are similar to the single-measurement meter, except that there are two input voltages in the dual-measurement meter amplifier. The two input terminals are connected to one signal source for experimental testing. From the simulation results in "Section 3.3", one can see that the frequency response of the dual-measurement meter is nearly the same as the single-measurement meter. Therefore, the experimental results of the dual-displacement measurement meter should be similar. Figures 23 and 24 show the measured gain and phase bold plots of the dual-displacement measurement meter. It is seen that the measured 3 dB frequency is about 10 kHz which meets the design requirement. The experimental results are nearly identical with the simulation results with PSpice, as shown in Figs. 17 and 18.

4.2 Laser check

The test is performed on a high-speed vertical machining center, which is equipped with a 24,000 rpm high-speed spindle. A laser checking unit is placed on the surface of the working table as shown in Fig. 25.

A comparison of the spindle equipped with only one displacement meter with the proposed new model is shown in Fig. 26. An additional laser report is also provided to prove the test results. This figure shows that there exists some discrepancy between measure 1 (single-displacement meter), and the laser curve. Measure 2 (dual-displacement meter) with this new model nearly matches the laser curve, which confirm an extremely perfect compensation.

4.3 Cutting report

Figure 27 shows a the main checking dimensions of working piece, the material is plastic mold tool steel, code DIN M-461 (GMP21M), and it is the most popular high grade mold steel; the hardness of raw material is HRC 38–42° [23]. A three-dimension simultaneous program with highest spindle speed is applied. The tools used as shown in Table 1, representing different working time of roughing, second rough cut, prefinish cut, and fine cut. Each sample had been done on the same machining tooling and program. The cutting performance presents a significant improvement of tolerance and its working time when the dual-measurement meters are applied. Table 2 show cutting report of all models. Take checking point "A", "B", and "E" as an example, tolerance in between the spindle equipped with PT-100 thermo coupler and dual-displacement meter shows a six times improvement. And it is better performance when comparing with a single meter, too. A DEA brand high-precision three-dimensional coordinate system is applied to check all samples as shown in Fig. 28.

5 Conclusion

The proposed new model discovers that the tolerance is better than the single-measurement meter design. The work piece cutting time is much shorter than the spindle equipped with PT-100 and a much better geometrical report is shown. It is a great quality improvement of the accuracy performance. This will greatly help to improve machining quality level and meet the requirement of HSM technology. Moreover, machine daily warm-up time is no longer require, it saves a lot of energy waste and increase significantly the productivity of machine.

Fig. 19 M-code sample

```
#define          KL_number_of_mesuring      K+100                    (14-1)
L ML_spindle_growth_pluse
 IFT
 L MG_marker_one
 R ML_spindle_growth_pluse
 ELSE
 L MG_marker_one
 S ML_spindle_growth_pluse
 ENDI

  LN      ML_spindle_growth_pluse
  ON       MG_machine_parameter_are_read                              (14-2)
  EMT

  PS       KL_Analog_input_3
  CM        9003
  PL       WG_SP_growth                                               (14-3)
  M_display_module_error(KG_error_module_9003)

  L        WG_SP_growth
  +        WL_sun_value                                               (14-4)
  =        WL_sun_value

  INC      BL_average

  L        BL_average
  <        KL_number_of_mesuring
  EMT

  L        K+0
  =        BL_average

  L        WG_SP_growth
  >        K+800
O[
  L        WG_SP_growth                                               (14-5)
  <        K-800
]
  CMT      Growth_comp_reset
  EMT

  L        WL_sun_value
  /        KL_number_of_mesuring                                      (14-6)
  =        WG_SP_RMS_growth

  L        WG_SP_RMS_growth
  X        K+1000
  /        K+1600                                                     (14-7)
  =        PN_W580_lag_error_compensation_Z

LBL Growth_comp_reset                                                 (14-8)

  L        K+0
  =        WL_sun_value

L MG_marker_one
= PN_error_spindle_growth_fault

EM
```

Where
(14-1) Define the checking sequence, sample is set 100 times each pulse width.
(14-2) Stop compensation when PLC is not started or CPU is receiving input.
(14-3) Analog signal processor in CPU.
(14-4) Output voltage summary.
(14-5) Reset after CPU receive every input.
(14-6) Voltage value counting (RMS).
(14-7) Voltage convert to be distance.
(14-8) Reset

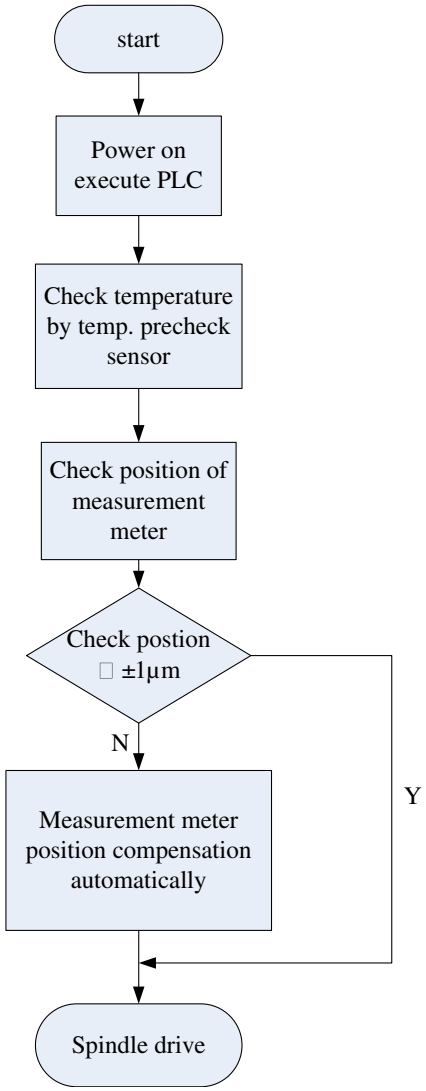

Fig. 20 Precheck flowchart

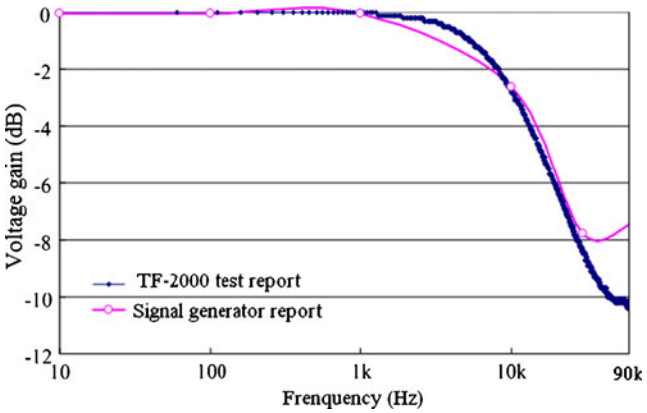

Fig. 21 Single-measurement meter voltage gain Bold polt

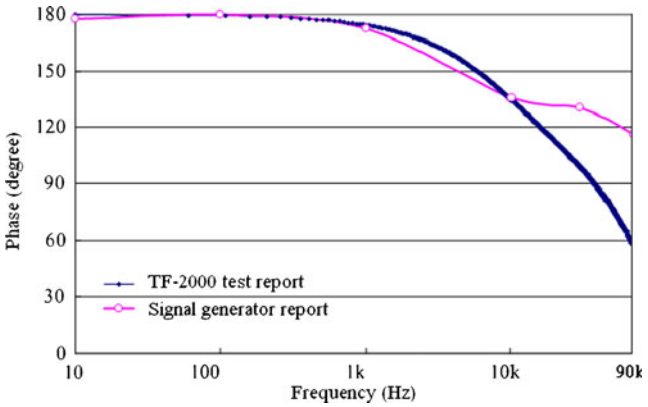

Fig. 22 Single-measurement meter phase Bold polt

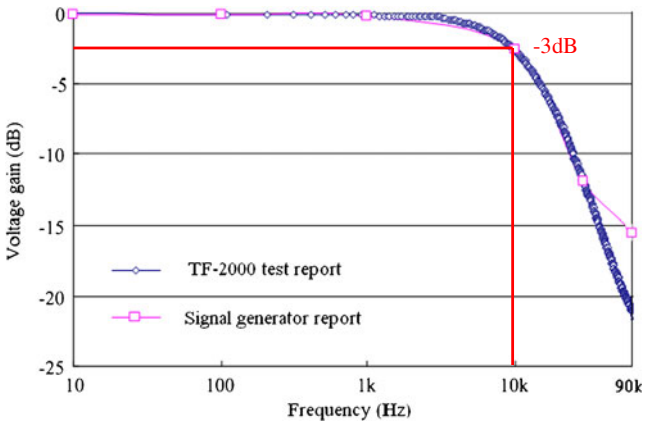

Fig. 23 Dual-measurement meter voltage gain Bold polt

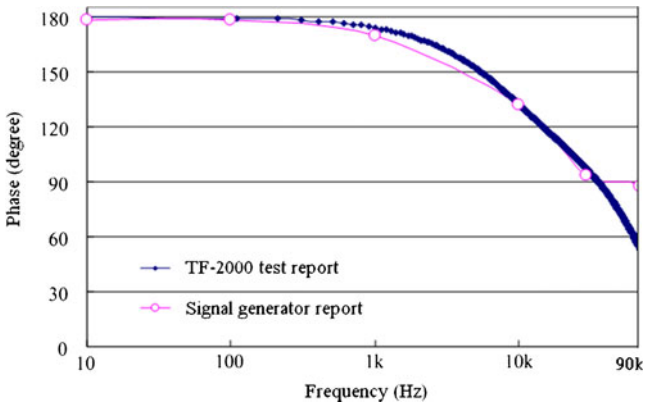

Fig. 24 Dual-measurement meter phase Bold polt

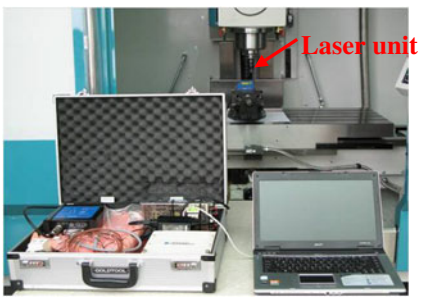

Fig. 25 Laser checking unit setup

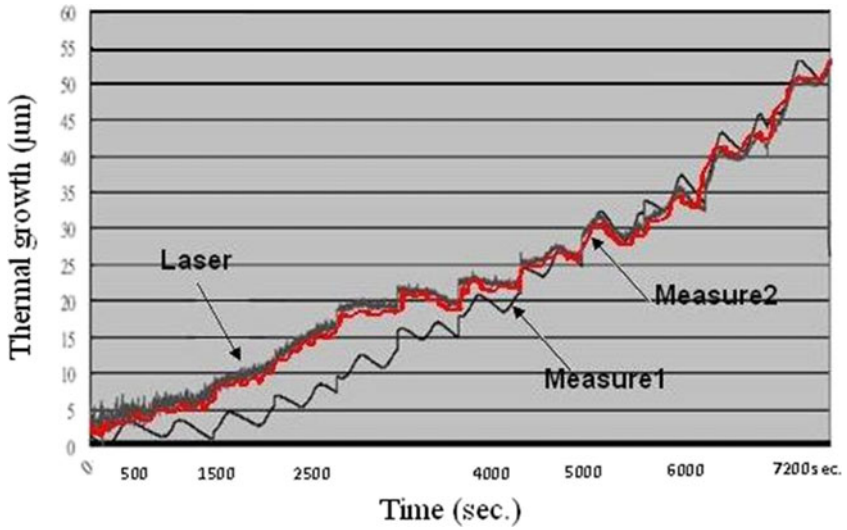

Fig. 26 Comparison curve of lasers and two models

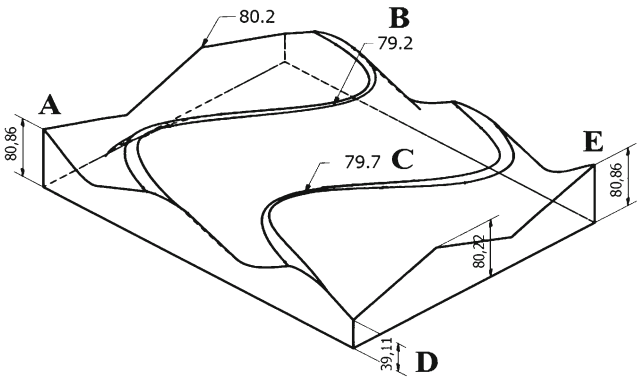

Fig. 27 Working piece and its main checking points

Table 1 Tools table

Program	Tool diameter (mm)	Total No. of edges in the tools	Working time PT-100 (min)	Working time single meter (min)	Working time dual meter (min)	Spindle speed (rpm)
Roughing	12	3	98′ 15″	98′ 15″	98′ 13″	2,000
Second Roughing	10	2	113′ 0″	113′ 0″	112′	4,000
Pre-finish	10	2	65′ 14″	56′ 25″	50′ 50″	5,500
Finishing	10	2	655′ 15″	610′ 30″	560′ 10″	6,000

All tools are Sandvik brand tools. Tool no.: R300-32T16-12M/R300-20A25C-10L/R216.44-10030-AK22N/R216.44-10030-AK22N

Table 2 Geometrical test report

	Check points and requirement	Spindle without compensation (tolerance)	Spindle with PT-100 (tolerance)	Spindle with single-measurement meter (tolerance)	Spindle with dual-measurement meter (tolerance)
A	80.86	80.24 (−0.62)	80.80 (−0.06)	80.85 (−0.01)	80.85 (−0.01)
B	79.20	78.60 (−0.60)	79.14 (−0.06)	79.20 (−0)	79.20 (−0)
C	79.70	79.05 (−0.65)	79.65 (−0.05)	79.69 (−0.01)	79.70 (−0)
D	39.11	38.50 (−0.65)	39.06 (−0.05)	39.11 (−0)	39.11 (−0)
E	80.86	80.20 (−0.66)	80.80 (−0.06)	80.84 (−0.02)	80.86 (−0)

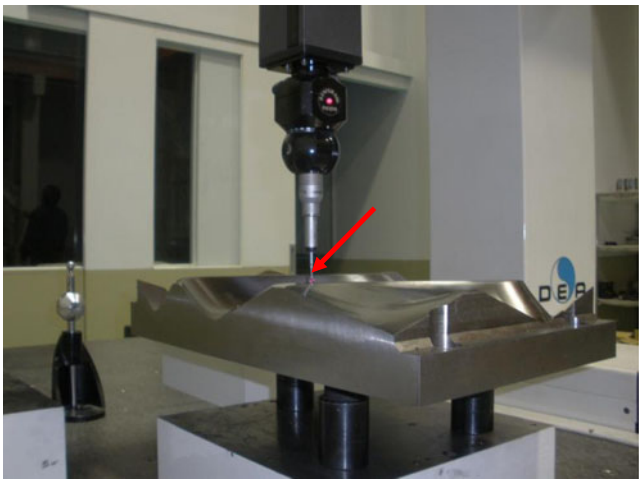

Fig. 28 Three-dimensional coordinate system

Acknowledgments The project is supported by the foundation for the Author of Excellent Doctoral Dissertation of Green Energy Technology Association of the Republic of China (project no. 201018).

References

1. Donmez A (2005) Smart machining systems. Manufacturing Engineering Laboratory, National Institute of Standards and Technology, www.mel.nist.gov/proj/sms.htm
2. Lin W, Jian Fu FC, Yu Qiang QL (2010) Speed optimization control method of smooth motion for high-speed CNC machine tools. Int J Adv Manuf Technol. doi:10.1007/s00170-009-2383-2
3. Zhang S, Li JF, Deng X, Li YS (2009) Investigation on diffusion wear during high-speed machining Ti-6A1-4V alloy with straight tungsten carbide tools. Int J Adv Manuf Technol 44:17–25. doi:10.1007/s00170-008-1803-z
4. Zone-Ching L, Jia-Shing C (2007) The building of spindle thermal displacement model of high speed machine center. Int J Adv Manuf Technol 34:556–566
5. Gomez-Acedo E, Olarra A, Lopez de la Calle LN (2012) A method for thermal characterization and modeling of large gantry-type machine tools. Int J Adv Manuf Technol. doi:10.1007/s00170-011-3879-0
6. Kim SM, Lee SK (2005) Spindle housing design parameter optimization considering thermo-elastic behavior. Int J Adv Manuf Technol 25:1061–1070
7. Chen JS, Hwang YW (2006) Centrifugal force induced dynamics of a motorized high-speed spindle. Int J Adv Manuf Technol 30:10–19. doi:10.1007/s00170-0005-0032-y
8. Chen J-S, Chen K-W (2005) Bearing load analysis and control of a motorized high speed spindle. Int J Mach Tool Manuf 45:1487–1493
9. Chen JS, Chiou G (1995) Quick testing and modeling of thermally induced errors of CNC machine tools. Int J Mach Tool Manuf 35 (7):1063–1074
10. Bossmanns Bernd Tu, Jay F (1999) A thermal model for high speed motorized spindles. Int J Mach Tool Manuf 39:1345–1366
11. Wong J (1986) Temperature measurements gain from advances in high-precision Op amps. Electronic Design
12. Wikimedia Foundation (2008) "Thermocouple". http//en.wikipedia.org
13. Simm A, Theodoulidis T, Poulakis N, Tian GY (2010) Investigation of the magnetic field response from eddy current inspection of defects. Int J Adv Manuf Technol. doi:10.1007/s00170-010-2915-5
14. NDT Resource Center (2008) Depth of penetration and current density. http://www.ndt-ed.org
15. Lee Neville KS, Chow Jacky KH, Chan Albert CK (2009) Design of precision measurement system for metallic hole. Int J Adv Manuf Technol 44:539–547
16. Ping Z, Nianjie M, Shuying G (2012) The research and application of intelligent multi-point displacement meter. CSIE LNEE 128:159–165
17. ACE CORP (2006) PU-03A*291-102 Sensor, Kanagawa Japan
18. Paton BE (1998) Sensors, transducers, & LabVIEW. National Instruments, Virtual Instrumentation, Canada
19. Kitchin C, Counts L (2006) A designer's guide to instrumentation amplifiers, 3rd edn. Analog Device Inc., North Wood
20. Phillips CL, Harbor RD (2000) Feedback control system, Forthth edn. Prentice Hall, New Jersey
21. Pallas-Areny R, Webster JG (1991) Sensors and signal conditioning. Wiley, New York
22. Mohan N, Undeland TM, Robbins WP (2003) Power electronics—converters, applications, and design, 3rd edn. Wiley, New Jersey
23. Jenkins GM, Watts DG (1968) Spectral analysis and its applications. Holden-Day, San Francisco
24. Floyd TL (2005) Electronics devices, conventional current version, 7th edn. Pearson Education, Upper Saddle River
25. Jensen JE, Tuttle WA, Stewart RB and Brechna H (1980) Brookhaven National Laboratory Selected Cryogenic Data Notebook, volume II. Brookhaven National Laboratory, Associated Universities, Inc.
26. Chrome molybdenum steel of Taiwan Hsin Ying chromium molybdenum steel. http://www.steel-heattreatment.com